ACS Photonics

Article

pubs.acs.org/journal/apchd5

Unique Hot Carrier Distributions from Scattering-Mediated Absorption

Jason Codrington,[†] Noor Eldabagh,[†] Kimberly Fernando,[†] and Jonathan J. Foley, IV*

Department of Chemistry, William Paterson University, 300 Pompton Road, Wayne, New Jersey 07470, United States

Supporting Information

ABSTRACT: Light-initiated generation of energetic carriers has attracted considerable attention as a paradigm for photocatalysis and solar energy conversion, and the use of noble metal nanoparticles that support localized surface plasmon resonances has been widely explored as a medium for realizing this paradigm. It was recently shown that composite nanostructures enabling the interplay between dielectric scattering resonances and broadband absorption in small metal nanostructures, a phenomenon termed scattering-mediated absorption, can be used to mediate energetic carrier transfer and selective photochemistry with low-intensity light while completely circumventing plasmon resonance. In this work, we develop a multiscale modeling approach for elucidating the hot carrier dynamics initiated by scattering-mediated absorption. Our calculations reveal that unique hot carrier distributions and dynamics arise from scattering-mediated absorption as compared to plasmon excitation and also suggest that in a variety of circumstances scattering-mediated absorption may lead to more efficient hot carrier generation compared to plasmon resonance under the same external illumination conditions. These results are an important first step in understanding the phenomena of scattering-mediated hot carrier generation, which has potential for expanding the palette of materials that can be utilized for hot carrier mediated photochemistry beyond plasmonic metals and for enabling unique pathways for photocatalytic transformations.

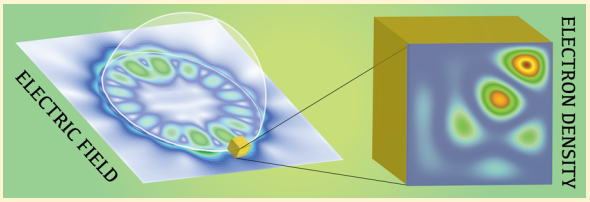

KEYWORDS: *hot carrier dynamics, nanoparticles, scattering-mediated absorption, plasmons*

Various strategies that exploit the optical properties of metal nanoparticles, namely, their ability to support localized surface plasmon resonances (LSPR), which are collective oscillations of their conduction electrons driven by light, have been explored recently with the aim of using low-intensity light to efficiently drive chemical reactions.[1−4] The interest in this area has been motivated partly by the fact that metal nanoparticles (most prominently silver and gold) are exceptionally good absorbers of visible light; therefore, they are ideal candidates for harvesting solar photons.[5] Importantly, the resonant properties of plasmonic particles are highly tunable by parameters under synthetic control such as geometry, composition, surface chemistry, and the surrounding environment.[6−8] An emerging paradigm that exploits LSPR for photocatalysis is known as plasmon-mediated hot-electron transfer (PHET), and a growing number of reports are demonstrating the ability of PHET to catalyze energetically demanding chemical reactions.[9−16]

In PHET, the collective plasmon excitation decays rapidly (on a 10 fs time scale) to a nonequilibrium distribution of energetic electron−hole pairs, or a so-called hot carrier distribution.[2,17−21] Hot carriers can deposit energy into reactive degrees of freedom of molecules adsorbed to the nanoparticle surface, thereby initiating chemical transformations. Despite the considerable progress made in demonstrating the potential of PHET, its widespread application faces several challenges. The intrinsic optical properties of noble metals that give rise to the extraordinarily large absorption cross sections associated with LSPR are also fundamentally related to the broad energy spectra and short lifetimes associated with LSPR and the subsequent hot carrier distributions.[22] Furthermore, the time scale of hot carrier relaxation competes with transfer to adsorbate states (both occur on 100 fs time scales), which fundamentally limits the efficiency of energy transfer.[19] Finally, there are a limited number of materials that show promising plasmonic behaviors (most prominently silver and gold), and it is desirable to extend the palette of available materials to include nonprecious metals and metals with broader applicability in catalysis.[15]

Considering this, an incredible opportunity exists to identify new classes of materials capable of mediating light−matter interactions and energy transfer events that offer the same advantages as metal nanoparticles, namely, exceptional light-harvesting potential, while also offering greater selectivity and efficiency in energy transfer, as well as tunable surface chemistry for enhanced catalytic activity. Ideally, such structures could be made mostly, if not entirely, from cost-effective materials. Recent progress toward this aim has been made by designing hybrid nanostructures that effectively delegate the light-harvesting and catalytic functions to separate components of the structure. Recently, Halas and co-workers demonstrated an antenna-reactor concept that leverages the near-field enhancement from aluminum plasmons to generate energetic carriers

Received: October 9, 2016
Published: January 24, 2017

DOI: 10.1021/acsphotonics.6b00773
ACS Photonics 2017, 4, 552−559

on palladium islands and showed the efficacy of this strategy for the photcatalytic transformation of acetylene to ethylene.[15] Two of the current authors, along with Sun and co-workers, demonstrated a phenomena known as scattering-mediated absorption (SMA), where dielectric scattering resonances in SiO_2 nanospheres were utilized to induce resonant absorption in nonplasmonic platinum nanoparticles in SiO_2/Pt nanohybrids.[13] The SMA phenomena was also observed to induce highly selective photocatalytic oxidation of benzyl alcohol to benzaldehyde.[13] Zhang et al. independently described an SMA phenomenon in Au-TiO_2 nanohybrids that leveraged so-called whispering gallery modes to enhance plasmonic and nonplasmonic absorption in gold nanoparticles and demonstrated these structures' efficacy for photocatalytic water splitting.[14] Interestingly, hot carrier transfer was implicated in the photocatalytic mechanisms that resulted from these SMA phenomena.[13,14] The prospect of using SMA in hybrid dielectric/metal nanostructures to initiate hot carrier generation and transfer is particularly compelling, as it could completely circumvent plasmon excitation. Not only does this open up possibilities to utilize a broad palette of earth-abundant and cost-effective materials, it also presents the possibility of realizing unique photocatalytic pathways owing to differences in the distributions and dynamics of energetic carriers produced by SMA compared to those produced by plasmon excitation.

The push to identify novel structures for mediating hot carrier generation and transfer has been paralleled by efforts to develop theoretical methodologies to elucidate these processes. The underlying metal electronic structure has been treated at levels ranging from free-electron models confined by potential wells[17,23−26] (here called "particle-in-a-well" (PIW) models) and the Jellium model within the local density approximation (Jellium LDA)[24] to atomistic density functional theory (DFT).[18,20,21,27] In totality, these theoretical investigations have yielded a number of valuable insights into the relative importance of particle geometry, material band structure, and electronic correlation effects on hot carrier generation in metal nanostructures. Using PIW models, Govorov and co-workers developed a theory of hot carrier generation within the framework of time-dependent perturbation theory that has elucidated a variety of shape- and size-dependent factors for optimizing the hot carrier generation.[17,23] A similar approach was also pursued by Kumarasinghe et al. suggesting that nanorods are exceptionally good structures for hot carrier generation.[25] García de Abajo and co-workers recently described a quantum master equation approach with an underlying PIW model that elucidated a number of key factors that influence hot carrier excitation and decay dynamics.[26] Nordlander and co-workers have directly compared free-electron and Jellium-LDA models and found that correlation effects within LDA have a negligible impact on hot carrier generation and dynamics arising from LSPR in Ag nanospheres as compared to geometric effects on the same.[24] The utilization of atomistic DFT by Sundararaman et al.,[18] Louie and co-workers,[27] and Brown et al.[21] has provided valuable insight into the role that metal band structure plays in determining the efficiency of hot carrier generation, the asymmetry between hot electron and hot hole generation, and the contributions to hot carrier relaxation. An important finding of these studies is that interband transitions play a dominant role in hot carrier generation in gold, but are much less important in silver due to the large energetic gap between the Fermi level and the d bands in silver.[18,20,21,27]

We developed a novel approach for studying hot carrier dynamics that may arise from arbitrary electromagnetic fields, including the unique near fields that arise from SMA on hybrid dielectric−metal nanoparticles and LSPR on noble metal nanoparticles. In our approach, we numerically solve the time-dependent Schrödinger equation within the configuration interaction singles (CIS) basis. The single-particle basis utilized in the CIS expansion corresponds to PIW energy eigenfunctions. Coulomb repulsion between the electrons is neglected in our current implementation; however, the CIS wave function is expanded in terms of antisymmetrized configurations, and so the many-electron dynamics obey the Pauli exclusion principle (see Supporting Information (SI) for more details). This approach can be considered a time-domain formulation of the PIW-based approaches described earlier.[17,23−25] Future extensions to include electron−electron repulsion and uniform nuclear charge would yield a time-domain formulation of the Jellium model within mean-field theory if the CIS basis were used or with higher-order treatment of electron−electron correlation if higher levels of excitation were included in the many-electron wave function. Such extensions could prove valuable for elucidating the role of correlation effects on electronic dynamics arising from SMA.

Importantly, our method goes beyond a perturbative inclusion of the electric field and enables us to follow the electronic degrees of freedom subject to strong fields with arbitrary time dependence, which are characteristic of SMA. Specifically, the explicit time dependence of this approach allows us to capture transitions that become important as the near fields from the scattering resonances continue to interact with the metal electrons for 10's to 100's of femtoseconds. Over these time scales, population accumulates in various excited configurations and transitions between different excited configurations become important to the dynamics. This is a unique feature of SMA that is likely unimportant in plasmonic generation of hot carriers due to the impulsive nature of the plasmon field. Although these transient field effects will not be relevant in photocatalytic applications, we anticipate that future work that combines the ability to treat transient effects with a more realistic description of the underlying electronic structure will be an important tool to use, particularly in conjunction with time-resolved spectroscopies, to provide further fundamental insight into energy transport and relaxation processes in composite structures that support SMA.

We consider the electronic degrees of freedom on the metal nanoparticle subject to the time-dependent Hamiltonian

$$\hat{H}(t) = \hat{H}_{\mathrm{el}} - \mathbf{E}(t)\cdot\hat{\mu} \tag{1}$$

where the specific form of $\mathbf{E}(t)$ derives from a rigorous time-domain electrodynamics calculation with a realistic model of the nanostructures in question and $\hat{H}_{\mathrm{el}}$ describes noninteracting electrons confined to metal nanocubes (NCs) by an infinite potential well. We compute the time-domain field using a commercial simulator based on the finite-difference time-domain (FDTD) method.[28] Incorporating $\mathbf{E}(t)$ from these FDTD simulations into the time-dependent Hamiltonian enables us to investigate the unique ways in which the electronic degrees of freedom evolve under the influence of the distinct time-varying fields that result from LSPR and from dielectric scattering resonances, allowing us a unique window into the hot carrier dynamics resulting from LSPR as compared to SMA. Further details on the FDTD simulations can be found in the SI.

DOI: 10.1021/acsphotonics.6b00773
ACS Photonics 2017, 4, 552−559

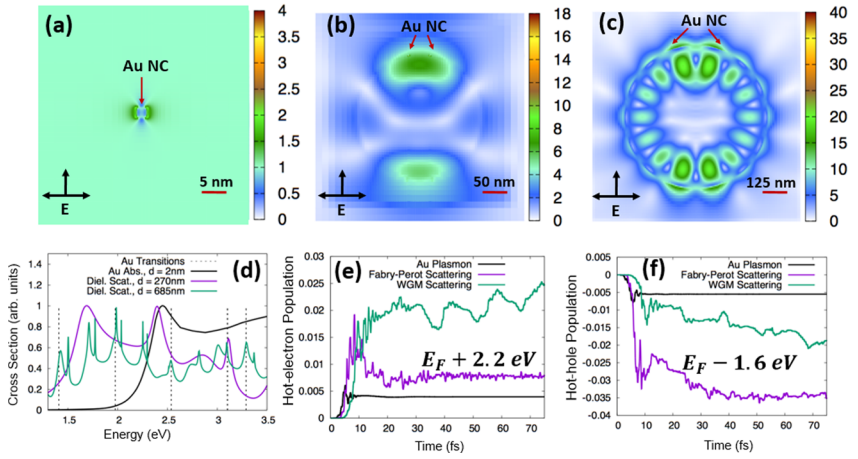

Figure 1. Three regimes for light−matter interactions leading to unique spatial and temporal shaping of the incident field and the corresponding impact on electronic dynamics in an L = 2 nm PIW Au nanocube. Plots of the near-field enhancements ($|\mathbf{E}|/|\mathbf{E}_0|$) are shown for the Au NC LSPR (λ = 532 nm, panel a), a Fabry−Perot resonance of a d = 270 nm dielectric nanosphere decorated with Au NCs (λ = 397 nm, panel b), and a whispering gallery mode resonance of a d = 685 nm dielectric nanosphere decorated with Au NCs (λ = 493 nm, panel c). The extinction spectra of these three structures are shown overlaid with the dipole-allowed transitions in the PIW model of the Au NC, showing particularly strong overlap between these transitions and the scattering resonances of the d = 685 nm dielectric nanosphere (panel d). The hot carrier populations $({}^1D_p^p(t) - {}^1D_p^p(t=0))$ are computed to measure hot electron and hot hole generation. Both dielectric scattering resonances show more efficient generation of hot electrons (panel e) and hot holes (panel f) compared to LSPR in this case.

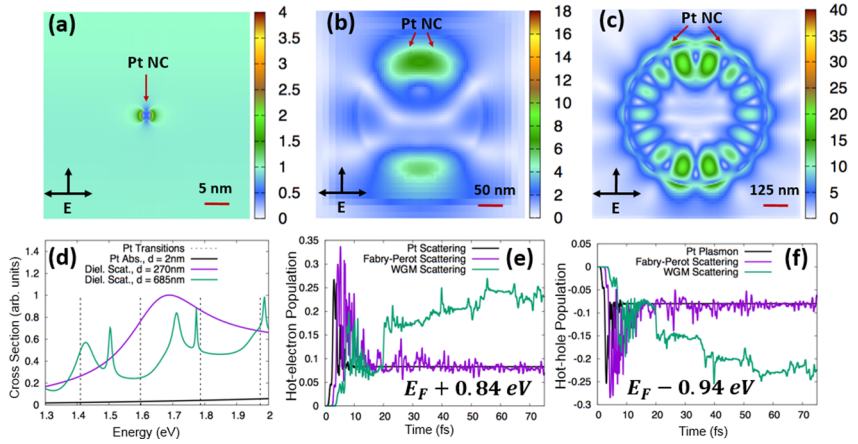

Figure 2. Three regimes for light−matter interactions leading to unique spatial and temporal shaping of the incident field and the corresponding impact on electronic dynamics in a L = 2 nm PIW Pt nanocube. Plots of the near-field enhancements ($|\mathbf{E}|/|\mathbf{E}_0|$) are shown of the Pt NC's extinction maximum (λ = 200 nm, panel a), a Fabry−Perot resonance of a d = 270 nm dielectric nanosphere decorated with Pt NCs (λ = 397 nm, panel b), and a whispering gallery mode resonance of a d = 685 nm dielectric nanosphere decorated with Pt NCs (λ = 493 nm, panel c). The extinction spectra of these three structures are shown overlaid with the dipole-allowed transitions in the PIW model of the Pt NC, showing partial overlap between these transitions and the scattering resonances of the d = 685 nm dielectric nanosphere (panel d). The change in orbital populations $({}^1D_p^p(t) - {}^1D_P^p(t=0))$ is computed to measure hot electron and hot hole generation. The WGM shows much more efficient generation of hot electrons (panel e) and hot holes (panel f) compared to FP resonance in this case.

The many-electron wave function of the metal nanoparticles is expanded in terms of a configuration-interaction expansion that includes all singly excited configurations,[29]

$$|\Psi_{\mathrm{CIS}}\rangle = c_0|\Phi_0\rangle + \sum_{i,a} c_i^a|\Phi_i^a\rangle \tag{2}$$

where the configuration $|\Phi_i^a\rangle$ has an electron excited from orbital i to orbital a, and c_0 and c_i^a are complex expansion coefficients. Unless otherwise specified, indices i, j indicate orbitals that are occupied in the ground-state reference configuration and indices a, b indicate orbitals that are unoccupied in the ground-state reference.

The time evolution of the wave function can be subsumed in the expansion coefficients, which allows the time-dependent Schrödinger equation to be written

$$i\hbar\frac{\mathrm{d}}{\mathrm{d}t}\mathbf{c}(t) = \mathbf{H}(t)\,\mathbf{c}(t) \tag{3}$$

where $\mathbf{c}(t)$ is the vector of complex expansion coefficients and $\mathbf{H}(t)$ is the time-dependent Hamiltonian matrix. The Hamiltonian matrix is composed of three unique classes of elements in the CIS model,

DOI: 10.1021/acsphotonics.6b00773
ACS Photonics 2017, 4, 552−559

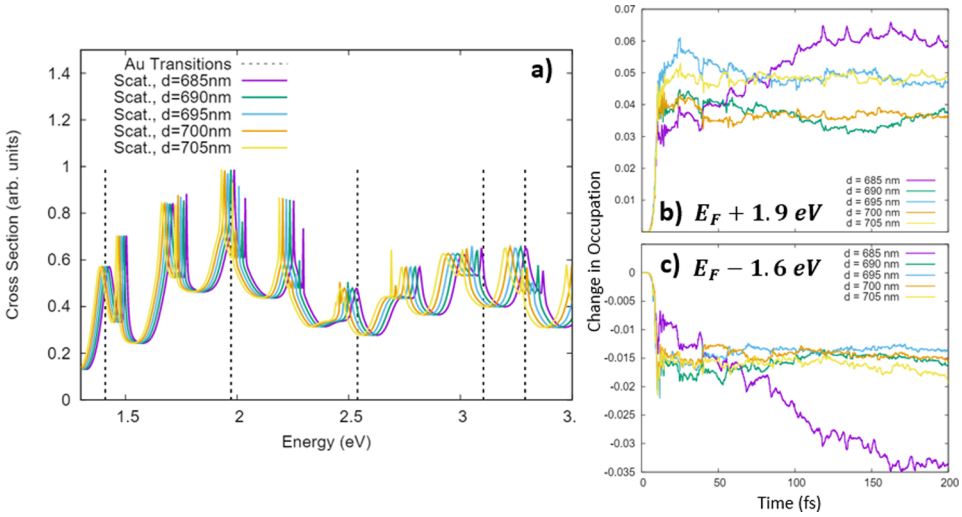

Figure 3. Fine-shaping of the spatial and temporal profile of the incident field through the geometry of the dielectric nanosphere. Panel a shows the scattering spectra of a size progression of dielectric nanospheres that display predominately whispering gallery mode visible resonances. The 685 nm nanosphere's scattering spectrum has the best overlap with the dipole-allowed transitions in the L = 2 nm PIW Au NC model, and this structure shows the most efficient generation of hot electrons in the most energetic orbitals included in our active space (panel b) and more efficient generation of hot holes in the lowest energy orbitals included in the PIW Au NC active space (panel c).

$$\mathbf{H}(t) = \begin{pmatrix} \langle \Phi_0 | \hat{H}(t) | \Phi_0 \rangle & \langle \Phi_0 | \hat{H}(t) | \Phi_i^a \rangle \\ \langle \Phi_j^b | \hat{H}(t) | \Phi_0 \rangle & \langle \Phi_j^b | \hat{H}(t) | \Phi_i^a \rangle \end{pmatrix} \tag{4}$$

Explicit expressions for each class of matrix elements are given in the SI. Importantly, the lower diagonal block of the CIS Hamiltonian matrix contains terms that couple together different excited configurations. In particular, transitions between singly excited configurations that differ in only one unoccupied index ($|\Phi_i^a\rangle \rightarrow |\Phi_i^b\rangle$) or that differ in only one occupied index ($|\Phi_i^a\rangle \rightarrow |\Phi_j^a\rangle$) are enabled by the terms in the lower diagonal block. Such excited-state to excited-state transitions are absent from linear response TDDFT and approaches that use time-dependent perturbation theory to first order, as these include only transitions between ground-state and singly excited configurations ($|\Phi_0\rangle \rightarrow |\Phi_i^b\rangle$).[17,30] The ($|\Phi_i^a\rangle \rightarrow |\Phi_i^b\rangle$) and ($|\Phi_i^a\rangle \rightarrow |\Phi_j^a\rangle$) are important in this context because the fields that arise from SMA continue to evolve on a long (>100 fs) time scale. On this time scale, population can accumulate in excited-state configurations, enabling the SMA fields to drive transitions between excited configurations as well as from the ground-state configuration (see the SI and Figure S4 for more details).

Given the simplicity of the underlying electronic Hamiltonian, the field-free Hamiltonian matrix is diagonal, and only the dipolar interaction of the nanoparticle with the external field can induce transitions among the electronic configurations; hence the treatment in this work neglects excited-state thermalization contributions from electron−electron scattering. The underlying simplicity of the Hamiltonian and single-particle basis set also precludes a description of the material-dependent band structure within this approach. In this work, we explore SMA involving Au and Pt nanoparticles, and we wish to emphasize that the band structure effects that are neglected in this work are expected to have an impact on the hot carrier distributions in both of these metals, as both have energetic gaps between the d band and the Fermi level that are smaller than energy components of the optical fields considered here. Examination of these two metals within our model still presents considerable value because it provides insight into hot carrier dynamics in two distinct regimes of the driving field, which includes a superposition of the plasmon and dielectric scattering fields. In particular, these regimes include (1) when the plasmon resonance and the dielectric scattering resonance overlap in energy with transitions in the quantum model (i.e., SMA involving Au; see Figure 1d) and (2) when only the dielectric scattering resonances overlap with quantum transitions (i.e., SMA involving Pt; see Figure 2d). We also choose Au and Pt because the SMA phenomenon has been experimentally demonstrated in both metals, including in the work by Sun and co-workers,[13] which considered SiO_2 nanospheres decorated with Pt nanoparticles of similar size to the particles considered here, and the work of Zhang et al.,[14] which considered TiO_2 nanospheres decorated with large Au nanoparticles. It has been shown that band structure effects have less of an impact on hot carrier dynamics in Ag nanoparticles due to the relatively large (>3 eV) gap between the d bands and the Fermi level,[24,31] and so analogous calculations have been performed on Ag-decorated nanospheres showing similar qualitative features to results with Au and Pt (see SI and Figure S3). Future work that simulates the long-time electronic dynamics while also capturing band structure and many-body effects would be valuable for further elucidating fundamental aspects of hot carrier dynamics driven by SMA. It is expected that both of these effects will play a role in the hot carrier dynamics in a variety of ways, including by changing the available excitation/transition channels by mixing of the single-particle states, by modifying the transition rates through modification of transition dipole moments, and by enabling thermalization of the excited carriers through electron−electron scattering.

Because of the diagonal nature of the field-free Hamiltonian, each configuration $|\Phi_i^a\rangle$ is an eigenfunction of the field-free Hamiltonian. This simplifies the interpretation of the electronic structure relative to the CIS wave function in quantum chemistry applications where electron repulsion is included in the Hamiltonian and the excited electronic eigenfunctions are linear combinations of singly excited configurations. The

DOI: 10.1021/acsphotonics.6b00773
ACS Photonics 2017, 4, 552−559

multiplication of the Hamiltonian matrix on the coefficient vector generates the gradient of the coefficient vector in time, and a variety of algorithms have been developed to use this information to propagate the wave function in time. Here we use a symplectic integrator described in ref 32. Propagation of the CIS wave function is referred to as the TDCIS method throughout.[33−35]

We analyze the hot carrier distribution and dynamics that result from SMA and LSPR excitation by computing the instantaneous populations of orbitals both above and below the Fermi level of the metal nanostructure. In our model, the orbitals are energy eigenstates of a one-electron Hamiltonian and have well-defined kinetic energy, and the orbital populations are given by the diagonal elements of the one-electron-reduced density matrix (1-RDM),

$$ {}^1D_q^q(t) = \langle \Psi(t)|\hat{a}_q^\dagger \hat{a}_q|\Psi(t)\rangle \tag{5} $$

where the second-quantized operator $\hat{a}_q^\dagger$ ($\hat{a}_q$) creates (kills) an electron in orbital q.[29] The hot carrier populations plotted in Figures 1 and 2 panels e and f are computed as ${}^1D_q^q(t) - {}^1D_q^q(t = 0)$, and similarly for the change in occupations plotted in Figure 3 panels b and c. The orbital indices can be uniquely mapped to the relevant orbital quantum numbers (n_x, n_y, n_z for the PIW NC model) so that the orbital energies can be readily computed (see SI for more details).

The TDCIS approach is applied to investigate hot carrier dynamics of L = 2 nm gold and platinum NCs that are (a) free-standing so that the dynamics are induced by optical resonances supported by the NC alone and (b) supported on various dielectric nanospheres so that the dynamics are also induced by time-evolving near fields arising from dielectric scattering resonance. We choose these metals because attachment of gold and platinum metal nanoparticles to various sized dielectric nanospheres has been experimentally demonstrated; future work will investigate similar phenomena with nonprecious metals. The electronic structures of these model NCs are distinguishable by their Fermi energies and the number of electrons: the Au NC model has a Fermi energy of 5.52 eV (compared to the bulk value of 5.53 eV) and 472 electrons, and the Pt NC model has a Fermi energy of 9.40 eV (compared to the bulk value of 9.75 eV) and 1104 electrons. In this work, 4900 singly excited configurations are included in $|\Psi_{CIS}\rangle$ for both Au and Pt NCs. Despite the large number of excited states included in our many-electron wave functions, the high degeneracy of the underlying dipole-allowed transitions leads to a relatively small number of visible spectroscopic lines for the Au (see Figure 1d) and Pt models (see Figure 2d).

The spectral flexibility of dielectric scattering resonances allows tuning to overlap with one or more of these transition energies via the nanosphere size; in contrast, for very small metal nanoparticles, the position of the LSPR is intrinsically related to the relative permittivity of the metal.[36] This is illustrated by plotting the scattering spectrum of a moderate-sized (d = 270 nm) and large (d = 685 nm) dielectric nanosphere and the absorption spectrum of a small (d = 2 nm) gold nanosphere all computed via Mie theory.[36] These Mie spectra are overlaid with the dipole-allowed transitions in our PIW model of the Au NC (see Figure 1d). The d = 270 nm dielectric nanosphere has a relatively broad scattering resonance (herein referred to as a Fabry−Perot (FP) resonance) that overlaps with a PIW Au NC transition at 3.1 eV, and a d = 685 nm dielectric nanosphere has narrow scattering resonances (whispering gallery modes (WGM)) that overlap with multiple transitions between 1.3 and 3.3 eV. The 2 nm Au nanosphere has a broad absorption peak associated with its LSPR that partially overlaps with a dipole-allowed transition in the PIW Au NC at 2.5 eV.

As proxies of the hot carrier dynamics in the Au NC, we plot the population dynamics of the highest and lowest energy orbitals in the Au NC active space, which lie 2.2 eV above and 1.6 eV below the Fermi energy, respectively (Figure 1e and f). Snapshots of the populations of all active orbitals in the Au NC model at various times are also provided in the SI (see Figure S1). We observe that the LSPR generates a relatively small population of hot carriers with field-driven dynamics that evolve on a short (10 fs) time scale. FP resonance in this case leads to significantly more efficient hot hole generation with field-driven dynamics that evolve on a moderate (50 fs) time scale (Figure 1f), while WGM resonances lead to considerably more efficient hot electron generation with field-driven dynamics that evolve on a much longer (200 fs) time scale (Figure 1e and Figure 3b). Another key distinction between the hot carrier density generated by the Au LSPR and by SMA is that the hot carrier density of the former is concentrated within 1 eV of the Fermi level, while SMA leads to appreciable density ±2 eV of the Fermi level (see Figure S1).

These differences can be attributed in part to the unique ways in which each resonant interaction simultaneously modulates the incident optical fields in space and time. An illustration of spatial confinement associated with each resonance can be seen in the electric field intensity maps at the resonance frequency for the Au LSPR (Figure 1a), FP resonance (Figure 1b), and WGM resonance (Figure 1c); all resonances lead to approximately 1 order of magnitude near-field enhancement in the vicinity of the Au NC. A progression of resonance lifetimes can be inferred from the extinction spectra of the Au LSPR, the FP resonance, and the WGM resonance, with the Au LSPR having the broadest extinction peak and the shortest lifetime and the WGM having the most narrow extinction peaks and longest lifetimes. These lifetimes determine the period of time that the metal electrons are being driven by enhanced near fields associated with the optical resonances, and the long lifetime associated with the WGM means that the near field that drives the metal electrons continues to evolve on a relatively long time scale compared to the electronic dynamics. Longevity of the evolution of the electric field resulting from dielectric scattering resonances is consistent with the longer period of population transfer from the Fermi level and below to higher unoccupied orbitals when compared with surface plasmon resonance of Au. The differences in these dynamics can be clearly seen in the time traces of the populations driven by the LSPR and FP resonance, which are virtually flat after 20 fs, compared to the populations driven by WGM resonances, which continue to grow over a period of 100 fs (see Figure 2e and f).

In contrast to Au, small Pt nanoparticles do not support LSPR at visible wavelengths (see Figure 2d), and consequently, we do not observe any overlap between an absorption resonance of the 2 nm Pt nanoparticle and the dipole-allowed transitions of our PIW Pt NC model. We also consider the same geometries of the dielectric nanospheres as before (d = 270 nm and d = 685 nm); the scattering resonances of the former have partial overlap with transitions in the PIW Pt NC model at 1.6 and 1.8 eV, and the resonances of the latter have partial overlap with transitions at 1.8, 1.8, and 1.95 eV. Again,

DOI: 10.1021/acsphotonics.6b00773
ACS Photonics 2017, 4, 552−559

the dielectric scattering resonances provide approximately an order of magnitude near-field enhancement in the vicinity of the Pt NC, while the near-field enhancement provided by the lone Pt nanoparticle is much smaller ($|\mathbf{E}|/|\mathbf{E}_0| \approx 2$ at $\lambda = 200$ nm, corresponding to the extinction maximum; see Figure 2a, b, and c). Due to its relatively weak optical interaction, scattering of the Pt nanoparticle does not lead to a large density of hot carriers; small populations of carriers are created near the Fermi energy (see Figure S2). These hot carriers can be attributed mostly to direct interaction with the incident pulse, which has a peak field strength of $E_0 \approx 614\,000\,000$ V/m (see SI for more details). SMA on the $d = 270$ nm nanosphere (NS) leads to generation of hot carriers within 1 eV of the Fermi energy with dynamics that persist for moderate (50 fs) time scales. The WGMs supported by the $d = 685$ nm dielectric NS show much greater efficiency in creating energetic carriers compared to the resonances of the $d = 270$ nm dielectric NS or the Pt nanoparticle. For example, WGMs supported by the $d = 685$ nm nanosphere are 3 times more effective at generating holes in the lowest lying orbital ($E_F - 1.6$ eV) and electrons in the highest lying orbital ($E_F + 0.84$ eV) in the PIW Pt NC active space as compared to FP resonance of the $d = 270$ nm NS (see Figure 2e and f). The hot carriers driven by WGM also show much more persistent dynamics and continue to evolve beyond 100 fs (see Figure 2e and f and Figure S2). Fairly rapid fluctuations in the hot carrier populations are observed in both Au and Pt nanoparticles at relatively short times for all three regimes; this presumably results from the broad distribution of energies in the optical fields that encounter the metal nanoparticles at early times combined with the density of available transition channels. By contrast, analogous calculations that have a lower density of transition channels through neglect of excited-state to excited-state transitions show smoother dynamics (see Figure S4).

To demonstrate the exquisite tunability of the dielectric scattering resonances and their commensurate impact on the electronic dynamics, we consider SMA by a series of five different Au-decorated dielectric nanospheres. This progression from $d = 705$ nm to $d = 685$ nm brings the dielectric scattering modes progressively into resonance with the dipole-allowed transition in the PIW Au NC (see Figure 3a). We observe efficient hot carrier generation from SMA in all of these structures, though SMA from the $d = 685$ nm structure leads to the most efficient generation of hot carriers in the highest and lowest energy orbitals in the Au NC active space (see Figure 3b and c), most likely owing to the strong overlap between the scattering resonances and the transitions in the Au NC.

In this work, we have developed a multiscale theoretical approach that utilizes time-domain electrodynamics to achieve a rigorous description of how light is shaped in space and time by interactions with complex nanostructured matter and bridges this information with a real time-dependent configuration interaction singles approach to electronic dynamics. Importantly, this method goes beyond a perturbative inclusion of the electric field and enables us to follow the electronic degrees of freedom subject to strong fields with arbitrary time dependence,[33−35] both of which are characteristic of the near fields resulting from the nanophotonics resonances that were explored in this work. The explicit inclusion of time-domain fields would also enable investigation of time-resolved spectroscopy experiments on similar structures, where the incident fields themselves may be shaped in space and time.

We have applied this methodology to the study of hot carrier generation in novel hybrid nanostructures consisting of large dielectric core structures decorated by metal nanoparticles that enable the interplay between scattering resonances in the core structure and broadband absorption in the metal nanoparticles, a phenomena known as scattering-mediated absorption. We have shown that scattering-mediated absorption can generate hot carriers while completely circumventing plasmonic resonance. This result points to the potential for realizing efficient hot carrier generation and transfer in nonprecious metals that are earth-abundant and cost-effective; future investigations that utilize more realistic models of the electronic structure will be performed to develop a more detailed understanding of factors that influence the efficiency of hot carrier generation in nonplasmonic or poor plasmonic metals. Additional developments that focus on a treatment of the optical properties of the metal that is self-consistent across the electrodynamics and quantum dynamics domains may also be valuable and will be explored. In principle, the dielectric function may be derived directly from electronic structure calculations of the metal nanoparticles, and so a self-consistent approach would include deriving the dielectric function from the same electronic structure model used for the hot carrier dynamics. Currently, the electrodynamics calculations are performed using bulk dielectric data for the metals of interest, though disparities from bulk behavior have been well documented for particles of this size.[22,37−39] Analogous calculations that utilize size-dependent corrections to dielectric function in the electrodynamics calculations suggest that the hot electron dynamics resulting from SMA may be sensitive to the size-dependent dielectric response of the metal nanoparticles involved, though the qualitative features of the hot carrier dynamics reported in this work are preserved upon inclusion of these corrections (see Figure S5). The overall similarity is likely due to the fact that the scattered field associated with the large dielectric structure plays the dominant role in driving the dynamics.

Our results also reveal that unique electronic dynamics can be realized by modulating the frequency and line width of the scattering resonances, which can be controlled by the size and/or refractive index of the dielectric structure. In particular, high quality factor scattering resonances (e.g., whispering gallery modes) can induce electronic dynamics that persist for hundreds of femtoseconds, while plasmonic resonance induces field-driven dynamics on a time scale of 10 fs. The ability to drive excited-state dynamics of hot carriers through tuning of these resonances may have important implications for improving the efficiency and selectivity of photocatalysis via hot carrier transfer, which can be severely limited by the rapid decay of energetic carriers resulting from plasmon resonances.

■ ASSOCIATED CONTENT

Supporting Information

The Supporting Information is available free of charge on the ACS Publications website at DOI: 10.1021/acsphotonics.6b00773.

Additional figures illustrating hot carrier distributions and dynamics, as well as details of the time-dependent configuration interaction singles method and the finite-difference time domain simulations (PDF)

DOI: 10.1021/acsphotonics.6b00773
ACS Photonics 2017, 4, 552−559

AUTHOR INFORMATION

Corresponding Author

*E-mail: foleyj10@wpunj.edu.

ORCID

Jonathan J. Foley IV: 0000-0001-8814-4444

Author Contributions

†J. Codrington, N. Eldabagh, and K. Fernando contributed equally to this work.

Notes

The authors declare no competing financial interest.

ACKNOWLEDGMENTS

This work was performed, in part, utilizing resources at the Center for Nanoscale Materials, a U.S. Department of Energy, Office of Science, Office of Basic Energy Sciences User Facility (contract no. DE-AC02-06CH11357). J.J.F. acknowledges the College of Science and Health and the Center for Research at William Paterson University for startup and summer support. J.C. and N.E. acknowledge the NSF-GS-LSAMP for support. K.F. acknowledges the WPU Center for Research for support.

REFERENCES

(1) Linic, S.; Christopher, P.; Ingram, D. B. Plasmonic-metal nanostructures for efficient conversion of solar to chemical energy. *Nat. Mater.* **2011**, *10*, 911−921.

(2) Kale, M. J.; Avanesian, T.; Christopher, P. Direct Photocatalysis by Plasmonic Nanostructures. *ACS Catal.* **2013**, *4*, 116−128.

(3) Zhou, N.; López-Puente, V.; Wang, Q.; Polavarapu, L.; Pastoriza-Santos, I.; Xu, Q.-H. Plasmon-enhanced light harvesting: applications in enhanced photocatalysis, photodynamic therapy and photovoltaics. *RSC Adv.* **2015**, *5*, 29076.

(4) Park, J. Y.; Kim, S. M.; Lee, H.; Nedrygailov, I. I. Hot-electron-mediated surface chemistry: toward electronic control of catalytic activity. *Acc. Chem. Res.* **2015**, *48*, 2475.

(5) Atwater, H. A.; Polman, A. Plasmonics for improved photovoltaic devices. *Nat. Mater.* **2010**, *9*, 205−213.

(6) Sun, Y.; Xia, Y. Shape-controlled synthesis of gold and silver nanoparticles. *Science* **2002**, *298*, 2176−2179.

(7) Burda, C.; Chen, X.; Narayanan, R.; El-Sayed, M. A. Chemistry and properties of nanocrystals of different shapes. *Chem. Rev.* **2005**, *105*, 1025−1102.

(8) Gramotnev, D. K.; Bozhevolnyi, S. I. Plasmonics beyond the diffraction limit. *Nat. Photonics* **2010**, *4*, 83−91.

(9) Christopher, P.; Xin, H.; Linic, S. Visible-light-enhanced catalytic oxidation reactions on plasmonic silver nanostructures. *Nat. Chem.* **2011**, *3*, 467−472.

(10) Marimuthu, A.; Zhang, J.; Linic, S. Tuning selectivity in propylene epoxidation by plasmon mediated photo-switching of Cu oxidation state. *Science* **2013**, *339*, 1590−1593.

(11) Mukherjee, S.; Libisch, F.; Large, N.; Neumann, O.; Brown, L. V.; Cheng, J.; Lassiter, J. B.; Carter, E. A.; Nordlander, P.; Halas, N. J. Hot Electrons Do the Impossible: Plasmon-Induced Dissociation of H2 on Au. *Nano Lett.* **2013**, *13*, 240−247.

(12) Li, Z.; Foley, J. J., IV; Peng, S.; Sun, C.-J.; Ren, Y.; Wiederrecht, G. P.; Gray, S. K.; Sun, Y. Reversible Modulation of Surface Plasmons in Gold Nanoparticles Enabled by Surface Redox Chemistry. *Angew. Chem.* **2015**, *127*, 9076−9079.

(13) Zhang, N.; Han, C.; Xu, Y.-J.; Foley, J. J., IV; Zhang, D.; Codrington, J.; Gray, S. K.; Sun, Y. Near-field dielectric scattering promotes optical absorption by platinum nanoparticles. *Nat. Photonics* **2016**, *10*, 473−482.

(14) Zhang, J.; Jin, X.; Morales-Guzman, P. I.; Yu, X.; Liu, H.; Zhang, H.; Razzari, L.; Claverie, J. P. Engineering the Absorption and Field Enhancement Properties of Au-TiO2 Nanohybrids via Whispering Gallery Mode Resonances for Photocatalytic Water Splitting. *ACS Nano* **2016**, *10*, 4496−4503.

(15) Swearer, D. F.; Zhao, H.; Zhou, L.; Zhang, C.; Robatjazi, H.; Martirez, J. M. P.; Krauter, C. M.; Yazdi, S.; McClain, M. J.; Ringe, E.; Carter, E. A.; Nordlander, P.; Halas, N. J. Heterometallic antenna-reactor complexes for photocatalysis. *Proc. Natl. Acad. Sci. U. S. A.* **2016**, *113*, 8916−8920.

(16) Sousa-Castillo, A.; Comesaña-Hermo, M.; Rodríguez-González, B.; Pérez-Lorenzo, M.; Wang, Z.; Kong, X.-T.; Govorov, A. O.; Correa-Duarte, M. A. Boosting Hot Electron-Driven Photocatalysis through Anisotropic Plasmonic Nanoparticles with Hot Spots in Au-TiO2 Nanoarchitectures. *J. Phys. Chem. C* **2016**, *120*, 11690−11699.

(17) Govorov, A. O.; Zhang, J.; Gun'ko, Y. K. Theory of photoinjection of Hot Plasmonic Carriers from Metal Nanostructures into Semiconductors and Surface Molecules. *J. Phys. Chem. C* **2013**, *117*, 16616−16631.

(18) Sundararaman, R.; Narang, P.; Jermyn, A. S.; Goddard, W. A., III; Atwater, H. A. Theoretical predictions for hot-carrier generation from surface plasmon decay. *Nat. Commun.* **2014**, *5*, 5788.

(19) Wu, K.; Chen, J.; McBride, J. R.; Lian, T. Efficient hot-electron transfer by a plasmon-induced interfacial charge-transfer transition. *Science* **2015**, *349*, 632.

(20) Ma, J.; Wang, Z.; Wang, L.-W. Interplay between plasmon and single-particle excitations in a metal nanocluster. *Nat. Commun.* **2015**, *6*, 10107.

(21) Brown, A. M.; Sundararaman, R.; Narang, P.; Goddard, W. A., III; Atwater, H. A. Nonradiative Plasmon Decay and Hot Carrier Dynamics: Effects of Phonons, Surfaces, and Geometry. *ACS Nano* **2016**, *10*, 957−966.

(22) Kraus, W. A.; Schatz, G. C. Plasmon resonance broadening in small metal particles. *J. Chem. Phys.* **1983**, *79*, 6130−6139.

(23) Zhang, H.; Govorov, A. O. Optical Generation of Hot Plasmonic Carriers in Metal Nanocrystals: The Effects of Shape and Field Enhancement. *J. Phys. Chem. C* **2014**, *118*, 7606−7614.

(24) Manjavacs, A.; Liu, J. G.; Kulkarni, V.; Nordlander, P. Plasmon-Induced Hot Carriers in Metallic Nanoparticles. *ACS Nano* **2014**, *8*, 7630−7638.

(25) Kumarasinghe, C. S.; Premaratne, M.; Bao, Q.; Agrawal, G. P. Theoretical analysis of hot electron dynamics in nanorods. *Sci. Rep.* **2015**, *5*, 12140.

(26) Saavedra, J. R. M.; Asenjo-Garcia, A.; García de Abajo, F. J. Hot-Electron Dynamics and Thermalization in Small Metallic Nanoparticles. *ACS Photonics* **2016**, *3*, 1637−1646.

(27) Bernardi, M.; Mustafa, J.; Neaton, J. B.; Louie, S. G. Theory and computation of hot carriers generated by surface plasmon polaritons in noble metals. *Nat. Commun.* **2015**, *6*, 7044.

(28) Lumerical Solutions, Inc., http://www.lumerical.com/tcad-products/mode/.

(29) Szabo, A.; Ostlund, N. S. *Modern Quantum Chemistry: Introduction to Advanced Electronic Structure Theory*, 1st ed.; McGraw-Hill, 1989.

(30) Zuehlsdorff, T. J.; Hine, N. D. M.; Spencer, J. S.; Harrison, N. M.; Riley, D. J.; Haynes, P. D. Linear-scaling time-dependent density-functional theory in the linear response formalism. *J. Chem. Phys.* **2013**, *139*, 064104.

(31) Narang, P.; Sundararaman, R.; Atwater, H. A. Plasmonic hot carrier dynamics in solid-state and chemical systems for energy conversion. *Nanophotonics* **2016**, *5*, 96−11.

(32) Sanz-Serna, J. M.; Portillo, A. Classical numerical integrators for wave-packet dynamics. *J. Chem. Phys.* **1996**, *104*, 2349−2355.

(33) Krause, P.; Klamroth, T.; Saalfrank, P. Time-dependent configuration-interaction calculations of laser-pulse-driven many-electron dynamics: Controlled dipole switching in lithium cyanide. *J. Chem. Phys.* **2005**, *123*, 074105.

(34) Greenman, L.; Ho, P. J.; Kamarchik, E.; Mazziotti, D. A.; Santra, R. Implementation of the time-dependent configuration-interaction singles method for atomic strong-field processes. *Phys. Rev. A: At., Mol., Opt. Phys.* **2010**, *82*, 023406.

(35) DePrince, A. E., III; Pelton, M.; Guest, J. R.; Gray, S. K. *Phys. Rev. Lett.* **2011**, *107*, 196806.

DOI: 10.1021/acsphotonics.6b00773
ACS Photonics 2017, 4, 552−559

(36) Bohren, C. F.; Huffman, D. R. *Absorption and Scattering of Light by Small Particles*; John Wiley and Sons, 1998.
(37) Peng, S.; McMahon, J. M.; Schatz, G. C.; Gray, S. K.; Sun, Y. Reversing the size-dependence of surface plasmon resonances. *Proc. Natl. Acad. Sci. U. S. A.* **2010**, *107*, 14530−14534.
(38) Scholl, J. A.; Koh, A. L.; Dionne, J. A. Quantum plasmon resonances of individual metallic nanoparticles. *Nature* **2012**, *483*, 421−427.
(39) Sun, Y.; Foley, J. J., IV; Peng, S.; Li, Z.; K, G. S. Interfaced metal heterodimers in the quantum size regime. *Nano Lett.* **2013**, *13*, 3958−3964.

DOI: 10.1021/acsphotonics.6b00773
ACS Photonics 2017, 4, 552−559